JOC Article

# Multiorbital Interactions during Acyl Radical Addition Reactions Involving Imines and Electron-Rich Olefins

Sara H. Kyne,[†] Carl H. Schiesser,*[,†] and Hiroshi Matsubara[‡]

*School of Chemistry, Bio21 Molecular Science and Biotechnology Institute, The University of Melbourne, Victoria 3010, Australia, and Department of Chemistry, Graduate School of Science, Osaka Prefecture University, Sakai, Osaka 599-8531, Japan*

*carlhs@unimelb.edu.au*

*Received August 19, 2007*

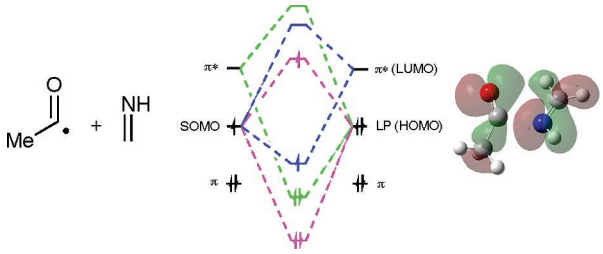


Ab initio and DFT calculations reveal that acyl radicals add to imines and electron-rich olefins through simultaneous SOMO → $\pi^*$, $\pi$ → SOMO, and HOMO → $\pi^*_{C=O}$ interactions between the radical and the radicalophile. At the CCSD(T)/aug-cc-pVDZ//QCISD/cc-pVDZ level, energy barriers of 15.6 and 17.9 kJ mol$^{-1}$ are calculated for the attack of the acetyl radical at the carbon and nitrogen ends of methanimine, respectively. These barriers are 17.1 and 20.4 kJ mol$^{-1}$ at BHandHLYP/cc-pVDZ. In comparison, barriers of 34.0 and 23.4 kJ mol$^{-1}$ are calculated at BHandHLYP/cc-pVDZ for reaction of the acetyl radical at the 1- and 2-positions in aminoethylene, repectively. Natural bond orbital (NBO) analysis at the BHandHLYP/6-311G** level of theory reveals that SOMO → $\pi^*_{imine}$, $\pi_{imine}$→ SOMO, and $LP_N$ → $\pi^*_{C=O}$ interactions are worth 90, 278, and 138 kJ mol$^{-1}$, respectively, in the transition state (**2**) for reaction of acetyl radical at the nitrogen end of methanimine; similar interactions are observed for the chemistry involving aminoethylene. These multiorbital interactions are responsible for the unusual motion vectors associated with the transition states involved in these reactions. NBO analyses for the remaining systems in this study support the hypothesis that the acetyl radical is ambiphilic in nature.

## Introduction

The construction of carbon−carbon and other bonds is central to organic chemistry and there are many reliable methods that can efficiently achieve these outcomes, involving both ionic and free-radical mediated chemistry. In the free-radical arena the literature abounds with examples for the construction of carbo- and heterocyclic compounds[1] and apart from examples that are affected by unusual orbital interactions,[2] the vast majority of these ring-closures involve intramolecular homolytic addition reactions that are governed by Beckwith−Houk considerations.[3,4]

Acyl radicals are convenient intermediates that can lead to the preparation of cyclic ketones, esters, and amides and are often generated from seleno- or telluro-esters.[5,6] Some examples of the synthetic utility of acyl radicals are shown in Scheme 1.[7−9]

* Address correspondence to this author. Phone: +61-3-8344-2432. Fax: +61-3-9347-8189.
[†] The University of Melbourne.
[‡] Osaka Prefecture University.

(1) Renaud, P.; Sibi, M. P. *Radicals in Organic Synthesis*; Wiley-VCH: Weinheim, Germany, 2001; Vols. 1 and 2.
(2) (a) Villar, F.; Kolly-Kovac, T.; Wquey, O.; Renaud, P. *Chem. Eur. J.* **2003**, *9*, 1566. (b) Corminboeuf, O.; Renaud, P.; Schiesser, C. H. *Chem. Eur. J.* **2003**, *9*, 1578. (c) Friestad, G. K.; Jiang, T.; Mathies, A. K. *Tetrahedron* **2007**, *63*, 3964.
(3) Beckwith, A. L. J.; Schiesser, C. H. *Tetrahedron* **1985**, *41*, 3925.
(4) Spellmeyer, D. C.; Houk, K. N. *J. Org. Chem.* **1987**, *52*, 959.
(5) Selenoester: Pfenninger, J.; Heuberger, C.; Graf, W. *Helv. Chim. Acta* **1980**, *63*, 2328.
(6) Telluroester: Chen, C.; Crich, D.; Papadatos, A. *J. Am. Chem. Soc.* **1992**, *114*, 8313.
(7) Boger, D. L.; Mathvink, R. J. *J. Org. Chem.* **1992**, *57*, 1429.
(8) Astley, M. P.; Pattenden, G. *Synlett* **1991**, 335.
(9) Crich, D.; Chen, C.; Hwang, J.; Yuan, H.; Papadatos, A.; Walter, R. I. *J. Am. Chem Soc.* **1994**, *116*, 8937.

10.1021/jo701825y CCC: $40.75 
Published on Web 12/19/2007

**SCHEME 1**

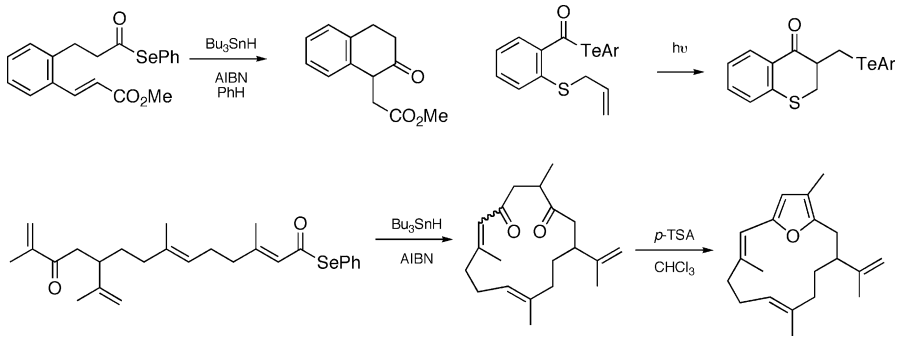


**SCHEME 2**

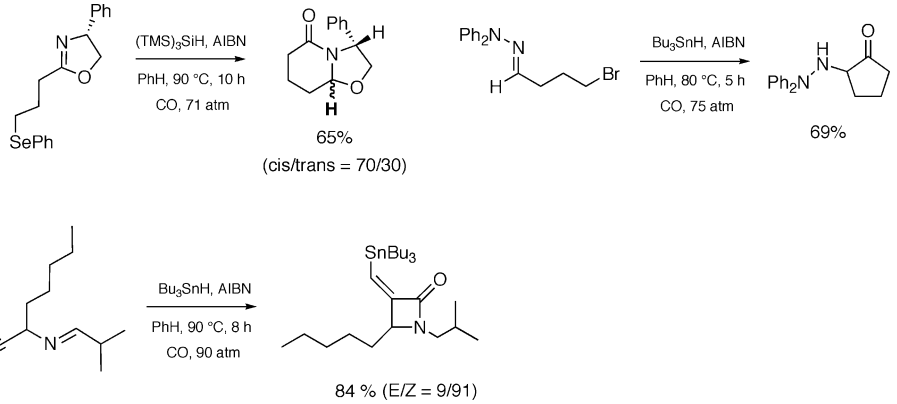


**SCHEME 3**

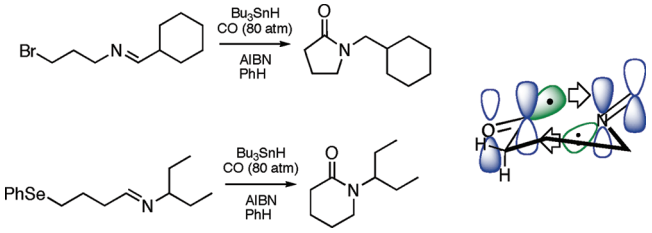


Recently, Ryu and co-workers developed carbonylation methodology for the generation of acyl radicals and showed that a multitude of ring systems could be constructed quickly and efficiently, examples of which are demonstrated in Scheme 2.[10−12] It should be noted that this chemistry overcomes many of the problems associated with the preparation of acyl radical precursors reported previously.[10]

During this work it was noted that acyl radicals are N-philic,[13] that is, they generally prefer to cyclize at the more electron-rich nitrogen end of C═N $\pi$-bonds (Scheme 3)[13,14] and computational investigations concluded that this outcome was in part the result of simultaneous SOMO → $\pi^*_{imine}$ and $LP_N$ → $\pi^*_{C=O}$ interactions operating between the two reacting units.[15−17] Given that alkyl radicals show little selectivity during cyclization onto imine $\pi$-bonds,[18] these multicomponent orbital interactions, interactions unavailable to alkyl radicals, play important roles in the chemistry of acyl radicals.

With our continued interest in acyl radicals, we became curious about the electronic demand posed by these radicals and whether or not selectivity would also be expected in the intermolecular counterparts to the chemistry described above. To the best of our knowledge, there are no examples of intermolecular reactions involving acyl radicals and imines. Furthermore, we were interested in exploring other $\pi$-systems that would be good candidates for exploiting multicomponent orbital interactions in synthesis.

We now report full details of this computational investigation and report that acyl radicals are ambiphilic in nature and can mask as electrophiles when confronted with electron-rich species that include imines and enamines.

## Results and Discussion

**Reaction of Acetyl Radical with Methanimine.** We began this investigation by examining the reaction of acetyl radical with methanimine, as representative examples of the key reacting components. Searching the $C_3H_6NO$ potential energy surface located structures **1** and **2** as the lowest energy transition states for reaction of the acetyl radical at the carbon and nitrogen ends of the C═N bond in methanimine, respectively (Scheme 4). Selected activation energy data (Scheme 4, $\Delta E_1^{\ddagger} - \Delta E_4^{\ddagger}$) are

(10) Schiesser, C. H.; Wille, U.; Matsubara, H.; Ryu, I. *Acc. Chem. Res.* **2007**, *40*, 303.
(11) Brinza, I. M.; Fallis, A. G. *J. Org. Chem.* **1996**, *61*, 3580.
(12) Ryu, I.; Miyazato, H.; Kuriyama, H.; Matsu, K.; Tojino, M.; Fukuyama, T.; Minakata, S.; Komatsu, M. *J. Am. Chem. Soc.* **2003**, *125*, 5632.
(13) Ryu, I.; Matsu, K.; Minakata, S.; Komatsu, M. *J. Am. Chem Soc.* **1998**, *120*, 5838.
(14) Tojino, M.; Otsuka, N.; Fukuyama, T.; Matsubara, H.; Ryu, I. *J. Am. Chem. Soc.* **2006**, *128*, 7712.
(15) Schiesser, C. H.; Matsubara, H.; Ritsner, I.; Wille, U. *Chem. Commun.* **2006**, 1067.
(16) Falzon, C. T.; Ryu, I.; Schiesser, C. H. *Chem. Commun.* **2002**, 2338.
(17) Matsubara, H.; Falzon, C. T.; Ryu, I.; Schiesser, C. H. *Org. Biomol. Chem.* **2006**, *4*, 1920.
(18) Bowman, W. R.; Stephenson, P. T.; Terett, N. K.; Young, A. R. *Tetrehedron Lett.* **1994**, *35*, 6369.

**TABLE 1. Calculated Energy Barriers[a] for the Forward ($\Delta E_1^{\ddagger}$, $\Delta E_3^{\ddagger}$) and Reverse ($\Delta E_2^{\ddagger}$, $\Delta E_4^{\ddagger}$) Reactions of Acetyl Radical with Methanimine and (Imaginary) Vibrational Frequencies ($\upsilon$)[b] of Transition States 1 and 2 (Scheme 4)**

| | $\Delta E_1^{\ddagger}$ | $\Delta E_1^{\ddagger}$ + ZPE | $\Delta E_2^{\ddagger}$ | $\Delta E_2^{\ddagger}$ + ZPE | $\upsilon$ | $\Delta E_3^{\ddagger}$ | $\Delta E_3^{\ddagger}$ + ZPE | $\Delta E_4^{\ddagger}$ | $\Delta E_4^{\ddagger}$ + ZPE | $\upsilon$ |
|---|---|---|---|---|---|---|---|---|---|---|
| UHF/6-311G** | 37.7 | 41.0 | 120.5 | 112.6 | 449i | 56.8 | 58.8 | 192.8 | 182.3 | 594i |
| MP2/6-311G** | 54.0 | 61.9 | 106.7 | 104.4 | 516i | 47.3 | 60.9 | 184.5 | 184.7 | 686i |
| BHandHLYP/6-311G** | 19.5 | 24.4 | 96.7 | 91.8 | 350i | 22.6 | 29.0 | 180.0 | 174.8 | 550i |
| BHandHLYP/cc-pVDZ | 17.1 | 22.4 | 100.9 | 96.2 | 361i | 20.4 | 27.0 | 181.9 | 176.5 | 547i |
| BHandHLYP/aug-cc-pVDZ | 19.6 | 24.5 | 100.5 | 95.5 | 330i | 24.1 | 30.9 | 181.0 | 175.2 | 509i |
| ROMP2/6-311G**// BHandHLYP/cc-pVTZ | 19.2 | | 71.4 | | | 29.8 | | 167.4 | | |
| QCISD/cc-pVDZ | 28.1 | 33.4 | 86.8 | 81.6 | 428i | 34.3 | 40.3 | 160.5 | 153.3 | 618i |
| CCSD(T)/aug-cc-pVDZ// MP2/aug-cc-pVDZ | 19.2 | | 81.9 | | | 23.0 | | 156.4 | | |
| G2//MP2(full)/6-31G* | 22.4 | | 69.7 | | | 18.2 | | 147.2 | | |
| B3LYP/6-311G** | 11.8 | 17.0 | 64.0 | 60.4 | 274i | 7.6 | 13.3 | 152.1 | 144.8 | 344i |
| B3LYP/cc-pVDZ | 8.3 | 14.1 | 68.6 | 65.4 | 289i | 4.9 | 10.5 | 155.3 | 148.1 | 342i |
| MPW1K/6-311G** | 9.3 | 14.2 | 97.2 | 92.9 | 274i | 10.9 | 17.5 | 190.2 | 184.8 | 452i |

[a] Energy in kJ mol$^{-1}$. [b] Frequencies in cm$^{-1}$.

**SCHEME 4**

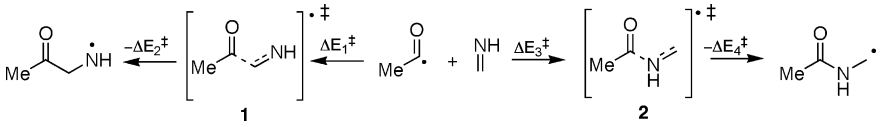


listed in Table 1, while a full listing at all levels of theory used in this study is available as Supporting Information (Table S1). Inspection of these tables reveals that at most levels of theory there is a slight preference for addition of the acetyl radical to the carbon end of the imine.

At the UHF/6-311G** level of theory the energy barriers are 37.7 and 56.8 kJ mol$^{-1}$ for the reaction proceeding through transition states **1** and **2**, respectively. Inclusion of electron correlation (MP2/6-311G**) serves to lower the predicted energy barrier to 47.3 kJ mol$^{-1}$ for the reaction involving **2**, but an increase to 54.0 kJ mol$^{-1}$ is observed for that involving **1**. At the QCISD/cc-pVDZ level of theory the activation energies of both transition states **1** and **2** are calculated to decrease to 28.1 and 34.3 kJ mol$^{-1}$, respectively. The BHandHLYP/cc-pVDZ and BHandHLYP/aug-cc-pVDZ levels of theory continue this trend, with the energy barriers calculated to be 17.1 and 19.6 kJ mol$^{-1}$ for transition state **1** and 20.4 and 24.1 kJ mol$^{-1}$ for transition state **2**. At the CCSD(T)/aug-cc-pVDZ//MP2/aug-cc-pVDZ level of theory, $\Delta E_1^{\ddagger}$ and $\Delta E_3^{\ddagger}$ are predicted to be 19.2 and 23.0 kJ mol$^{-1}$, respectively.

It is interesting to note that of the non-DFT methods, only G2//MP2(full)/6-31G* provides data that suggest a slight preference for acyl radical attack at the nitrogen end of the methanimine, with energy barriers of 22.4 ($\Delta E_1^{\ddagger}$) and 18.2 kJ mol$^{-1}$ ($\Delta E_3^{\ddagger}$). These data are to be compared with values of 32 and 50 kJ mol$^{-1}$ for methyl radical addition at the carbon and nitrogen ends of methanimine, respectively, using G2//MP2-(full)/6-31G*.[19] Clearly, the acetyl radical has a significantly greater preference for addition to nitrogen than does the methyl radical and this preference can be understood through application of Natural Bond Orbital (NBO) analysis (vide infra). Despite this, all calculations predict that the acetyl radical is essentially unselective in its reaction with methanimine, as opposed to the methyl radical, which is predicted to react exclusively at the carbon end of the C=N bond.

The data in Tables 1 and S1 also indicate that BHandHLYP performs as well as higher correlation techniques (CCST(T), QCISD) and therefore methods incorporating BHandHLYP are used extensively throughout the rest of this work. On the other hand, the B3LYP (Density Functional) method produces $\Delta E_1^{\ddagger}$ data that converge to values of about 8−12 (transition state **1**) and 5−8 (transition state **2**) kJ mol$^{-1}$, which are approximately 10 to 15 kJ mol$^{-1}$ less than the highest correlated levels of theory employed. Both B3LYP and MPW1K/6-311G** provide data that are significantly different from those obtained at other levels of theory. These sorts of differences for radical reactions calculated by using B3LYP and MPW1K have been noted before and, as we have previously suggested, we urge the use of caution when using these methods for calculating the energies of radical species.[15,17,20,21]

Table 1 also shows that the calculated energy barriers for the reverse reactions (Scheme 4, $\Delta E_2^{\ddagger}$, $\Delta E_4^{\ddagger}$) are substantially different for fragmentation at the two ends of the carbon−nitrogen bond. At the BHandHLYP/aug-cc-pVDZ level of theory these energy barriers are calculated to be 100.5 and 181.0 kJ mol$^{-1}$ for transition states **1** and **2**, respectively. Clearly there is substantial preference for the forward reaction in both cases; however, the energy barrier is also significantly lower for fragmentation of the product radical through transition state **1** when compared to **2** and this is a reflection on the relative stabilities of nitrogen versus carbon-centered radicals.

The transition states for attack at both ends of the imine are displayed in Figure 1, along with important geometrical features at selected levels of theory. A complete list is available as Supporting Information (Table S2). Motion arrows associated with the transition state vector in each case are included and give insight into the attack trajectory of the acetyl radical during addition to the imine.[21] The transition state separations are observed to be larger for attack at the carbon end of the imine

(19) Boyd, S. L.; Boyd, R. J. *J. Phys. Chem. A* **2001**, *105*, 7096.

(20) Morihovitis, T.; Schiesser, C. H.; Skidmore, M. A. *J. Chem. Soc., Perkin Trans. 2* **1999**, 2041.

(21) Lingwood, M.; Hammond, J. R.; Hrovat, D. A.; Mayer, J. M.; Borden, W. T. *J. Chem. Theory Comput.* **2006**, *2*, 740.

(22) BHandHLYP/6-311G** GaussView generated animations of the transition state vectors in **1** and **2** are available in the Supporting Information as Audio Video Interleave (AVI) files.

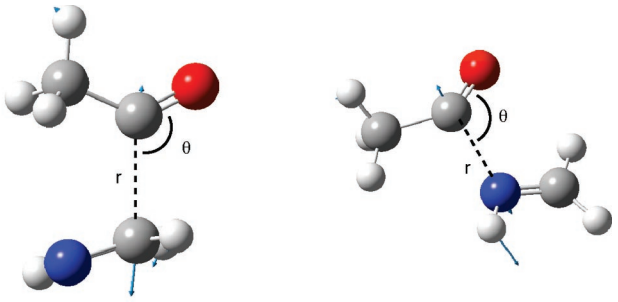


| | r | θ | | r | θ |
|---|---|---|---|---|---|
| BHandHLYP/6-311G** | 2.180Å | 118.2° | BHandHLYP/6-311G** | 1.940Å | 110.2° |
| BHandHLYP/cc-pVDZ | 2.188Å | 119.2° | BHandHLYP/cc-pVDZ | 1.935Å | 109.8° |
| QCISD/cc-pVDZ | 2.143Å | 119.7° | QCISD/cc-pVDZ | 1.928Å | 112.0° |

**FIGURE 1.** Selected optimized structures of transition states **1** and **2** involved in the homolytic addition of acetyl radical to methanimine (Scheme 4).

bond, with transition state **1** predicted to have separations between about 2.13 and 2.24 Å, compared to transition state **2** with separations of 1.76−2.08 Å. In addition the angles ($\theta$) located around the carbonyl bond are predicted to be slightly larger for attack at the carbon end of the imine $\pi$ system. At the BHandHLYP/6-311G** level of theory the angles for transition states **1** and **2** are calculated to be 118.2° and 110.2°, respectively.

Natural Bond Orbital (NBO) analysis at the BHandHLYP/6-311G** level of theory was carried out for both transition states. In the case of addition to the carbon end of the imine (transition state **1**), this analysis reveals SOMO → $\pi^*_{imine}$ and $\pi_{imine}$ → SOMO interactions (Figure 2, left). The former interaction, calculated to be worth 196 kJ mol$^{-1}$, is evident in the α spin-set, with the latter interaction evident in the $\beta$ spin-set and calculated to contribute 110 kJ mol$^{-1}$ (Figure 2, **1a** and **1b**). The nitrogen lone pair (calculated to be the HOMO) is orientated in such a manner as to make itself unavailable for bonding, and therefore does not contribute to the developing bonding interactions when the acetyl radical attacks the carbon

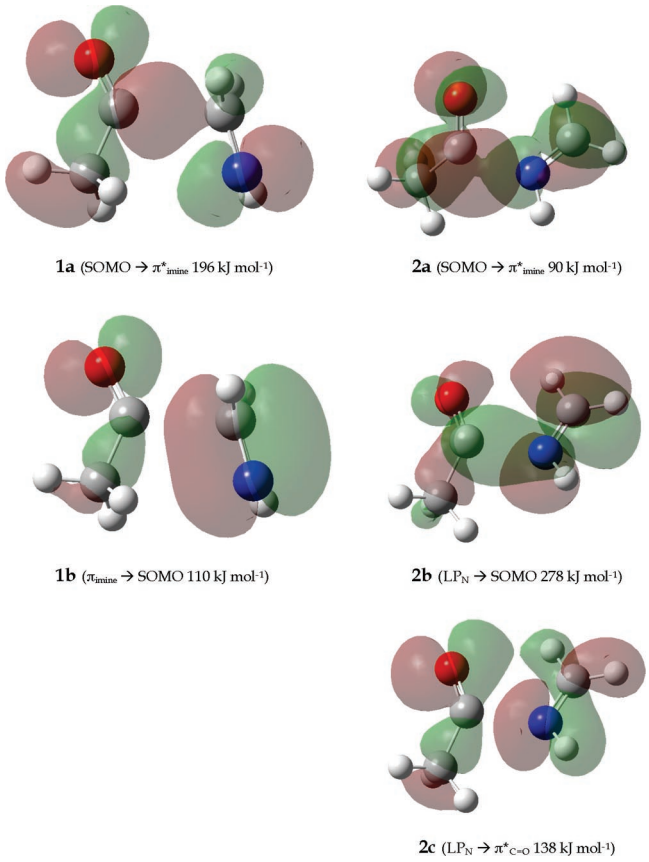


**FIGURE 3.** BHandHLYP/6-311G** optimized Kohn−Sham orbitals for the homolytic addition of acetyl radical to methanimine in transition states **1** and **2**.

end of methanimine. With the SOMO → $\pi^*_{imine}$ interaction larger than the $\pi_{imine}$ → SOMO interaction, we can conclude that in its reaction at the carbon end of the imine the acetyl radical acts predominantly as a nucleophilic radical. Visualization of the Kohn−Sham orbitals generated at the same level of theory depicts the overlap of the two reacting units in transition state **1** (Figure 3, left).

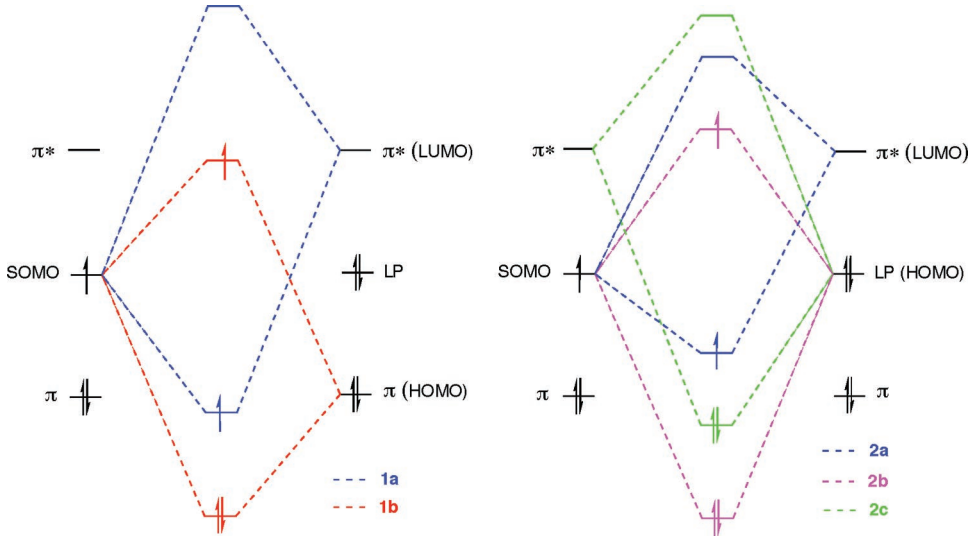


**FIGURE 2.** Energy profile diagram for NBO analysis of orbital interactions for the homolytic addition of acetyl radical to methanimine in transition states **1** (left) and **2** (right).

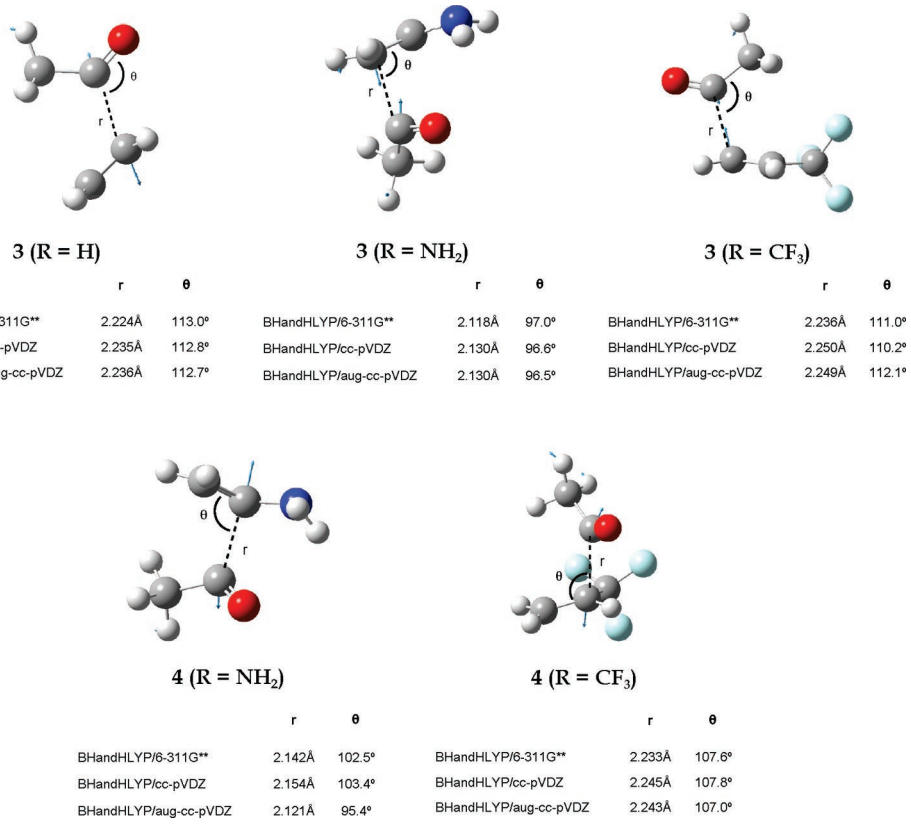


**FIGURE 4.** BHandHLYP/aug-cc-pVDZ optimized structures of transition states **3** and **4** for the homolytic addition of acetyl radical to ethylene, aminoethylene, and 3,3,3-trifluoropropene.

**TABLE 2. Calculated Energy Barriers[a] for the Forward ($\Delta E_1^{\ddagger}$, $\Delta E_3^{\ddagger}$) and Reverse ($\Delta E_2^{\ddagger}$, $\Delta E_4^{\ddagger}$) Reactions of Acetyl Radical with Ethylene, Aminoethylene, and Trifluoropropene and (Imaginary) Vibrational Frequencies ($\upsilon$)[b] of Transition States 3 and 4 (Scheme 5)**

| | $\Delta E_1^{\ddagger}$ | $\Delta E_1^{\ddagger}$ + ZPE | $\Delta E_2^{\ddagger}$ | $\Delta E_2^{\ddagger}$ + ZPE | $\upsilon$ | $\Delta E_3^{\ddagger}$ | $\Delta E_3^{\ddagger}$ + ZPE | $\Delta E_4^{\ddagger}$ | $\Delta E_4^{\ddagger}$ + ZPE | $\upsilon$ |
|---|---|---|---|---|---|---|---|---|---|---|
| R = H | | | | | | | | | | |
| BHandHLYP/6-311G** | 30.4 | 33.2 | 110.9 | 104.2 | 394i | | | | | |
| BHandHLYP/cc-pVDZ | 27.9 | 30.7 | 115.3 | 108.7 | 382i | | | | | |
| BHandHLYP/aug-cc-pVDZ | 29.7 | 32.6 | 115.1 | 108.5 | 377i | | | | | |
| R = $NH_2$ | | | | | | | | | | |
| BHandHLYP/6-311G** | 24.6 | 30.2 | 114.0 | 108.1 | 514i | 38.2 | 41.0 | 90.0 | 83.6 | 544i |
| BHandHLYP/cc-pVDZ | 23.4 | 28.5 | 120.1 | 114.1 | 502i | 34.0 | 36.7 | 92.6 | 86.2 | 527i |
| BHandHLYP/aug-cc-pVDZ | 23.5 | 29.0 | 116.8 | 111.2 | 476i | 38.9 | 42.3 | 95.0 | 89.0 | 571i |
| R = $CF_3$ | | | | | | | | | | |
| BHandHLYP/6-311G** | 18.0 | 20.9 | 108.8 | 104.3 | 354i | 29.5 | 31.3 | 101.2 | 95.8 | 378i |
| BHandHLYP/cc-pVDZ | 14.6 | 17.6 | 112.9 | 108.7 | 342i | 25.9 | 27.8 | 105.4 | 100.0 | 364i |
| BHandHLYP/aug-cc-pVDZ | 19.9 | 22.2 | 114.3 | 109.3 | 328i | 31.7 | 33.6 | 106.2 | 100.8 | 374i |

[a] Energy in kJ $mol^{-1}$. [b] Frequencies in $cm^{-1}$.

**SCHEME 5**

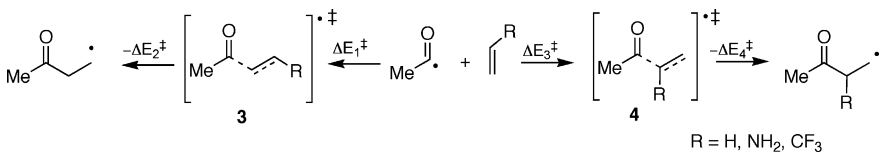


In comparison, NBO analysis for attack of the acetyl radical at the nitrogen end of the imine reveals a SOMO → $\pi^*_{imine}$ interaction worth 90 kJ $mol^{-1}$ in the α spin-set (Figure 2, **2a**). However, unlike attack at the carbon end of the imine, a strong interaction between the unpaired acetyl radical (SOMO) and the lone pair on nitrogen (imine HOMO) is observed in the $\beta$ spin-set. The latter interaction is calculated to be approximately three times larger than the SOMO → $\pi^*_{imine}$ interaction (278 kJ $mol^{-1}$, Figure 2, **2b**). Consequently, these data suggest that the acetyl radical is acting predominantly as an electrophilic radical in its reactions with the imine at the nitrogen end of the $\pi$ bond. Of significance is the calculation of a third strong interaction involving the nitrogen lone pair and the $\pi^*$ orbital of the carbonyl $\pi$-system. This secondary interaction is apparent in both the α and $\beta$ spin-sets, and is responsible for the unusual transition state motion vectors in transition state **2** (Figure 2, **2c**).[21] Inspection of the Kohn−Sham orbital associated with this interaction reveals these secondary interactions complement the

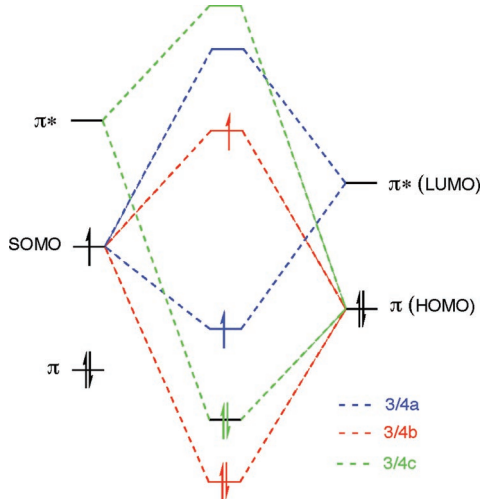


**FIGURE 5.** Interaction diagram showing possible orbital interactions during the homolytic addition of acetyl radical to ethylene, aminoethylene, and 3,3,3-trifluoropropene in transition states **3** and **4**.

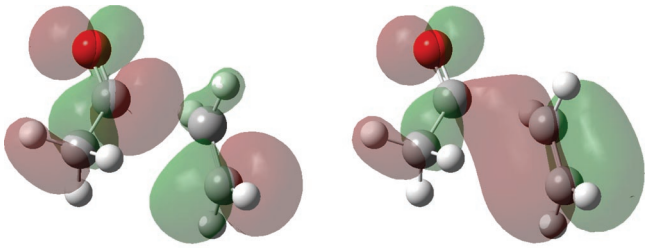

**3a**(H) (SOMO → $\pi^*_{alkene}$ 157 kJ mol$^{-1}$) **3b**(H) ($\pi_{alkene}$ → SOMO 144 kJ mol$^{-1}$)

**FIGURE 6.** BHandHLYP/6-311G** optimized Kohn−Sham orbitals in transition state **3** (R = H) for the homolytic addition of acetyl radical to ethylene.

primary radical interactions and exist in order to derive maximum energy gain from the available orbitals (Figure 3, right).

**Reactions of Acyl Radicals with Alkenes.** To further probe the electron demand in reactions involving acyl radicals, we next turned our attention to the reaction of the acetyl radical with ethylene and substituted alkenes of varying electron demand that include aminoethylene and 3,3,3-trifluoropropene (Scheme 5). As the previous benchmarking study had established that the BHandHLYP method seemed to provide reliable data for this chemistry, we chose to use this method in this study.

Searching of the relevant potential energy surfaces located transition state structures **3** and **4** for the addition to the two ends of the alkene. The calculated energy barriers for the forward ($\Delta E_1^{\ddagger}$, $\Delta E_3^{\ddagger}$) and reverse ($\Delta E_2^{\ddagger}$, $\Delta E_4^{\ddagger}$) reactions (Scheme 5) and (imaginary) transition state vibrational frequencies are listed in Table 2, while Figure 4 depicts the optimized transition structures **3** and **4** together with selected geometric data.

Inspection of Table 2 reveals that at the BHandHLYP/aug-cc-pVDZ level of theory the energy barriers for the forward and reverse reactions involving ethylene are 29.7 and 115.1 kJ mol$^{-1}$, respectively. Clearly there is substantial preference for the reaction leading to the product in this case. The motion arrows associated with transition state **3** (R = H) (Figure 4) reveal no unusual transition state motion, and this is perhaps not unexpected.

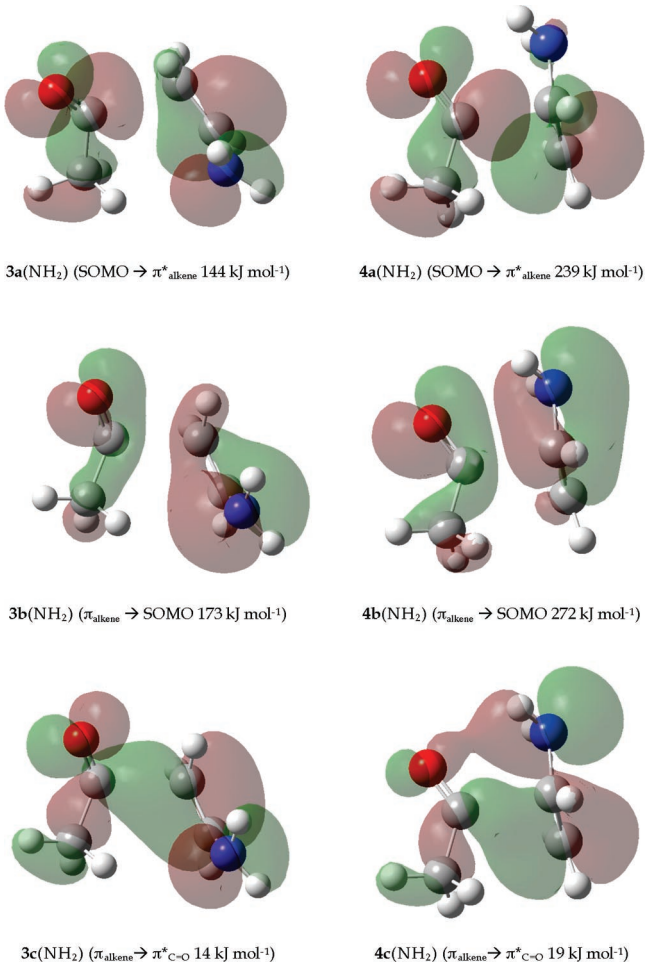

**3a**($NH_2$) (SOMO → $\pi^*_{alkene}$ 144 kJ mol$^{-1}$) **4a**($NH_2$) (SOMO → $\pi^*_{alkene}$ 239 kJ mol$^{-1}$)

**3b**($NH_2$) ($\pi_{alkene}$ → SOMO 173 kJ mol$^{-1}$) **4b**($NH_2$) ($\pi_{alkene}$ → SOMO 272 kJ mol$^{-1}$)

**3c**($NH_2$) ($\pi_{alkene}$→ $\pi^*_{C=O}$ 14 kJ mol$^{-1}$) **4c**($NH_2$) ($\pi_{alkene}$→ $\pi^*_{C=O}$ 19 kJ mol$^{-1}$)

**FIGURE 7.** BHandHLYP/6-311G** optimized Kohn−Sham orbitals and NBO calculated interaction energies for the homolytic addition of acetyl radical to aminoethylene in transition states **3** and **4** (R = $NH_2$).

However, with an electron-donating group present, as in the case of aminoethylene (R = $NH_2$), we begin to observe the "rocking" motion that we saw for **2**. Table 2 now reveals that the calculated activation energies for the forward addition reaction (Scheme 5, $\Delta E_1^{\ddagger}$) are consistently lower for attack at the carbon remote from the substituent (transition state **3**) at the various levels of theory employed in this study. At the BHandHLYP/aug-cc-pVDZ level of theory, addition to this end of the $\pi$ bond, with $\Delta E_1^{\ddagger}$ calculated to be 23.5 kJ mol$^{-1}$, is more than 15 kJ mol$^{-1}$ lower than that of its counterpart ($\Delta E_3^{\ddagger}$), indicating a slight preference in product distribution.

Inclusion of the electron-withdrawing substituent (R = $CF_3$), while revealing a similar energy trend (Table 2), is not associated with a transition state with unusual motion vectors (Figure 4). It should be noted that compared to ethylene, both donating and withdrawing groups reduce the energy barrier for attack at the carbon remote from the substituent, suggesting that the acetyl radical has ambiphilic tendencies.

NBO analyses were performed at the BHandHLYP/6-311G** level of theory on transition states **3** and **4**. Inspection of the NBO data reveals interactions between the acetyl radical (SOMO) and the alkene $\pi$ system (Figure 5), as well as, in the case of aminoethylene, of further interactions. For the reaction involving ethylene, the SOMO → $\pi^*_{alkene}$ interaction, calculated to be worth 157 kJ mol$^{-1}$, is apparent in the α spin-set, with a contribution of 144 kJ mol$^{-1}$ in the $\beta$ spin-set from the $\pi_{alkene}$

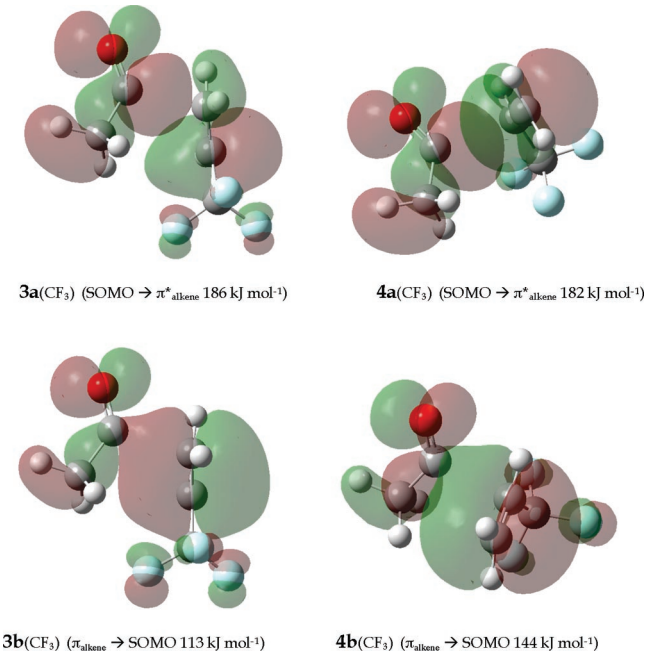


**FIGURE 8.** BHandHLYP/6-311G** optimized Kohn−Sham orbitals and NBO calculated interaction energies for the homolytic addition of acetyl radical to 3,3,3-trifluoropropene in transition states **3** and **4** (R = $CF_3$).

→ SOMO interaction (Figure 6). The acetyl radical is predicted to be essentially ambiphilic, or very slightly nucleophilic, in its reaction with ethylene. Visualization of the Kohn−Sham orbitals generated at the BHandHLYP/6-311G** level of theory allows us to observe the "traditional" transition state for homolytic addition to a $\pi$ system (Figure 6). The conformation assumed in the transition state is orientated in such a way as to allow optimum overlap of the radical SOMO with the alkene $\pi$ bond.

NBO analyses at the BHandHLYP/6-311G** level of theory were also carried out for transition states **3** and **4**, for the reaction involving aminoethylene (R = $NH_2$), with these analyses revealing interactions between the unpaired acetyl radical (SOMO) and the alkene $\pi$ and $\pi^*$ orbitals (Figure 7). In the case of addition to the carbon remote from the amine group (transition state **3**), the SOMO → $\pi^*_{alkene}$ interaction, calculated to be worth 144 kJ $mol^{-1}$, is evident in the α spin-set (Figure 7, **3a**, R = $NH_2$), with the $\pi_{alkene}$ → SOMO interaction evident in the $\beta$ spin-set and calculated to contribute 173 kJ $mol^{-1}$ (Figure 7, **3b**, R = $NH_2$). A third interaction between the $\pi^*$ orbital of the carbonyl $\pi$ system and the alkene $\pi$ orbital ($\pi_{alkene}$ → $\pi^*_{C=O}$), calculated to be worth a total (α + $\beta$) of 14.1 kJ $mol^{-1}$, is observed in both the α and $\beta$ spin-sets, and is responsible for the slight rocking motion in transition state **3** (Figure 7, **3c**, R = $NH_2$). The same trend is observed for acetyl radical addition to the carbon adjacent to the substituent. The $\pi_{alkene}$ → SOMO interaction evident in the $\beta$ spin-set is once again calculated to be larger than the SOMO → $\pi^*_{alkene}$ interaction apparent in the α spin-set (239 kJ $mol^{-1}$ vs 272 kJ $mol^{-1}$). Here, the third interaction ($\pi_{alkene}$ → $\pi^*_{C=O}$) is once again observed, calculated to contribute 19 kJ $mol^{-1}$ (Figure 7, **4c**, R = $NH_2$). In both instances the acetyl radical is observed to act predominantly as an electrophilic radical in its reaction with the aminoethylene.

NBO analysis of the dominant interactions in the transition states involved in the addition of acetyl radical to 3,3,3-trifluoropropene reveals a significantly larger contribution from the radical SOMO interaction than in the previous examples. At the BHandHLYP/6-311G** level of theory the transition state SOMO → $\pi^*_{alkene}$ interaction (**3a**, 186 kJ $mol^{-1}$; **4a**, 182 kJ $mol^{-1}$) observed in the α spin-set is calculated to be larger than the $\pi_{alkene}$ → SOMO interaction (**3b**,113 kJ $mol^{-1}$; **4b**, 144 kJ $mol^{-1}$) observed in the $\beta$ spin-set (Figure 8). We conclude that in its reaction with the trifluoromethyl-substituted olefin, the acetyl radical acts predominately as a nucleophilic radical.

## Conclusions

This computational study has shown that that acyl radicals add to imines and electron-rich olefins through simultaneous SOMO → $\pi^*$, $\pi$ → SOMO, and HOMO → $\pi^*_{C=O}$ interactions between the radical and the radicalophile. These multiorbital interactions are responsible for the unusual motion vectors associated with the transition states involved in these reactions. Natural bond orbital analyses on the transition states involved in this study provide quantitative information relating to these multicomponent interactions. These data support the hypothesis that the acetyl radical is ambiphilic in nature. We are currently further exploring this orbital phenomenon in other free-radical systems and will report the results of these studies in due course.

## Computational Methods

Ab initio and DFT molecular orbital calculations were carried out on Dell PowerEdge 400SC and TX7/i9510 Itanium 2 computers, using the Gaussian 03 program.[23] Geometry optimizations were performed with standard gradient techniques at the SCF, MP2, QCISD, BHandHLYP, B3LYP, and MPW1K levels of theory, using restricted and unrestricted methods for closed- and open-shell systems, respectively. In every case, standard basis sets were used. All ground and transition states were verified by vibrational frequency analysis. Further single-point QCISD and CCSD(T) calculations were performed on some of the MP2, BHandHLYP, and B3LYP optimized structures. When correlated methods were used, calculations were carried out by using the frozen core approximation. Values of $\langle s^2 \rangle$ never exceeded 0.86 before annihilation of quartet contamination (except for some UHF calculations) and were mostly 0.80 at correlated levels of theory. Where appropriate, zero-point vibrational energy (ZPE) corrections have been applied. Natural Bond Orbital (NBO) Analyses were carried out with NBO 5.0[24] linked through the Gaussian 03 program.

Optimized geometries and energies for all transition structures in this study (Gaussian Archive entries) are available as Supporting Information.

**Acknowledgment.** This work would not have been possible without the generous support of the Australian Research Council

(23) Frisch, M. J.; Trucks, G. W.; Schlegel, H. B.; Scuseria, G. E.; Robb, M. A.; Cheeseman, J. R.; Montgomery, J. A., Jr.; Vreven, T.; Kudin, K. N.; Burant, J. C.; Millam, J. M.; Iyengar, S. S.; Tomasi, J.; Barone, V.; Mennucci, B.; Cossi, M.; Scalmani, G.; Rega, N.; Petersson, G. A.; Nakatsuji, H.; Hada, M.; Ehara, M.; Toyota, K.; Fukuda, R.; Hasegawa, J.; Ishida, M.; Nakajima, T.; Honda, Y.; Kitao, O.; Nakai, H.; Klene, M.; Li, X.; Knox, J. E.; Hratchian, H. P.; Cross, J. B.; Adamo, C.; Jaramillo, J.; Gomperts, R.; Stratmann, R. E.; Yazyev, O.; Austin, A. J.; Cammi, R.; Pomelli, C.; Ochterski, J. W.; Ayala, P. Y.; Morokuma, K.; Voth, G. A.; Salvador, P.; Dannenberg, J. J.; Zakrzewski, V. G.; Dapprich, S.; Daniels, A. D.; Strain, M. C.; Farkas, O.; Malick, D. K.; Rabuck, A. D.; Raghavachari, K.; Foresman, J. B.; Ortiz, J. V.; Cui, Q.; Baboul, A. G.; Clifford, S.; Cioslowski, J.; Stefanov, B. B.; Liu, G.; Liashenko, A.; Piskorz, P.; Komaromi, I.; Martin, R. L.; Fox, D. J.; Keith, T.; Al-Laham, M. A.; Peng, C. Y.; Nanayakkara, A.; Challacombe, M.; Gill, P. M. W.; Johnson, B.; Chen, W.; Wong, M. W.; Gonzalez, C.; Pople, J. A. *Gaussian 03*, Revision B.05; Gaussian, Inc.: Pittsburgh, PA, 2003.

(24) Glendening, E. D.; Badenhoop, J. K.; Reed, A. E.; Carpenter, J. E.; Bohmann, J. A.; Morales, C. M.; Weinhold, F. *NBO 5.0*; Theoretical Chemistry Institute: University of Wisconsin, Madison, WI, 2001.

through the Centers of Excellence Program. We also gratefully acknowledge the support of the Victorian Institute for Chemical Sciences High Performance Computing Facility and the Library and Science Information Center, Osaka Prefecture University.

**Supporting Information Available:** Table S1 and Gaussian Archive entries for the optimized transition structures (**1**−**4**) and higher level calculated single-point energies and BHandHLYP/6-311G** GaussView generated animations of the transition state vectors in **1** and **2** as Audio Video Interleave (AVI) files. This material is available free of charge via the Internet at http://pubs.acs.org.

JO701825Y